Monitoring the Reflectivity Calibration of a Scanning Radar Using a Profiling Radar and a Disdrometer

CHRISTOPHER R. WILLIAMS

Cooperative Institute for Research in Environmental Sciences, University of Colorado, and NOAA/Aeronomy Laboratory, Boulder, Colorado

KENNETH S. GAGE

NOAA/Aeronomy Laboratory, Boulder, Colorado

WALLACE CLARK

Cooperative Institute for Research in Environmental Sciences, University of Colorado, and NOAA/Aeronomy Laboratory, Boulder, Colorado

PAUL KUCERA

Department of Atmospheric Sciences, University of North Dakota, Grand Forks, North Dakota

(Manuscript received 4 May 2004, in final form 17 November 2004)

ABSTRACT

This paper describes a method of absolutely calibrating and routinely monitoring the reflectivity calibration from a scanning weather radar using a vertically profiling radar that has been absolutely calibrated using a collocated surface disdrometer. The three instruments have different temporal and spatial resolutions, and the concept of upscaling is used to relate the small resolution volume disdrometer observations with the large resolution volume scanning radar observations. This study uses observations collected from a surface disdrometer, two profiling radars, and the National Weather Service (NWS) Weather Surveillance Radar-1988 Doppler (WSR-88D) scanning weather radar during the Texas–Florida Underflight-phase B (TEFLUN-B) ground validation field campaign held in central Florida during August and September 1998.

The statistics from the 2062 matched profiling and scanning radar observations during this 2-month period indicate that the WSR-88D radar had a reflectivity 0.7 dBZ higher than the disdrometer-calibrated profiler, the standard deviation was 2.4 dBZ, and the 95% confidence interval was 0.1 dBZ. This study implies that although there is large variability between individual matched observations, the precision of a series of observations is good, allowing meaningful comparisons useful for calibration and monitoring.

1. Introduction

The development in the early 1990s of a fully operational national network of Weather Surveillance Radar-1988 Doppler (WSR-88D) radars, also known as the Next Generation Radar (NEXRAD) network (Heiss et al. 1990; Baer 1991; Crum et al. 1993, 1998), has paved the way for a major advancement in the ability to provide quantitative precipitation estimates (QPEs) over most of the continental United States (Serafin and Wilson 2000; Smith et al. 1996). While this capability has led to a major improvement in operational nowcasting and short-range forecasting, it is widely recognized that there is still room for substantially improving the retrieval of precipitation estimates from WSR-88D radars (Glitto and Choy 1997; Baeck and Smith 1998; Serafin and Wilson 2000). Among the principal factors that affect the quality of QPEs are radar calibration, the variability of the vertical profile of reflectivity (VPR), range-dependent sampling issues, and the empirical Z–R relationships used to relate radar reflectivity to rain rate. The Z–R relations have been found to vary substantially depending on the vari-

Corresponding author address: Christopher R. Williams, CIRES–NOAA/Aeronomy Lab, Mail Stop R/AL 3, 325 Broadway, Boulder, CO 80305.
E-mail: Christopher.R.Williams@noaa.gov

ability of drop size distributions (DSDs) within the evolution of the storm (Brandes et al. 1999) and from location to location (Austin 1987; Atlas et al. 1995). The use of polarimetric radar will improve QPEs (Brandes et al. 2002), yet polarimetric observations will not be operationally available for several years to come.

Clearly, given the current reliance on the Z–R relationship to retrieve precipitation estimates from observed reflectivity, it is essential that the scanning radar be well calibrated. The calibration of the individual WSR-88D radars has recently been shown to vary as much as a few dBZ in relation to the National Aeronautics and Space Administration (NASA) Tropical Rainfall Measuring Mission (TRMM) precipitation radar (PR) (Atlas 2002; Anagnostou et al. 2001; Bolen and Chandrasekar 2000). Furthermore, comparisons of reflectivities from adjacent WSR-88D radar reflectivities in the contiguous United States differ by as much as a few decibels (Smith et al. 1996). Such differences can lead to substantial systematic errors in precipitation estimates (Ulbrich and Lee 1999). Consistent calibration between adjacent network radars is also crucial for constructing radar mosaics used in real-time weather forecasting. In this paper, we focus attention on the radar calibration issue and develop a methodology for using profilers to calibrate scanning radars and to monitor their calibration. The use of profilers to calibrate scanning radars was first outlined in Gage et al. (2000), and this paper develops a methodology that produces statistics from 2 months of profiling and scanning radar observations.

While sophisticated approaches are currently used to calibrate each WSR-88D radar, the calibration problem remains to be fully solved (Atlas 2002). There are many techniques in use today for verification of WSR-88D radar calibrations, including routine engineering measurements of the various subsystems (Serafin and Wilson 2000), and a very different approach that combines the radar calibration and Z–R relationships through the comparison of radar-derived rain maps with dense networks of rain gauges (e.g., Stellman et al. 2001; Anagnostou et al. 1999; Smith et al. 1996). Along the lines of this paper, direct comparisons of reflectivities from the WSR-88D radars with surface Joss–Waldvogel disdrometers (JWDs) have been utilized by Martner (1977) and Ulbrich and Miller (2001). However, the volume and space–time mismatches between the surface disdrometers and scanning radars add large uncertainties to these comparisons. Further, sampling issues that lead to underestimation of DSD and rainfall by disdrometers when only a few raindrops are detected are discussed by Smith et al. (1993).

In this study, we utilize a vertically pointing radar profiler to provide a statistical transfer standard between the disdrometer and the scanning radar. The surface disdrometer is used to calibrate the collocated profiler, and the calibrated profiler provides a reflectivity transfer standard at multiple altitudes that may be compared directly and routinely with the reflectivities observed by a nearby scanning radar observing over the disdrometer/profiler site.

The fundamental problem with comparing reflectivities from the surface disdrometer, the profiling radar, and the scanning radar is that all three instruments have different spatial and temporal resolutions. This would not be a problem if the precipitation was not varying in time and space. But since precipitation is variable at different temporal and spatial resolutions, the uncertainties of the QPE from each instrument will be a combination of the instrument measurement error and the spatiotemporal variability of the precipitation.

This paper presents a comparison of scanning radar observations from the WSR-88D radar in Melbourne, Florida (KMLB), with those from two profiling radars deployed in central Florida during the TRMM Texas–Florida Underflight-phase B (TEFLUN-B) ground validation field campaign in August and September 1998. The KMLB radar observations have been used by NASA for TRMM ground validation since the launch of the *TRMM* satellite in November 1997 and are the subject of several related studies (Anagnostou and Krajewski 1998, 1999a,b). The results discussed here confirm the study of Anagnostou et al. (2001), finding that the KMLB radar was well calibrated during the TEFLUN-B campaign. The statistics from this study also indicate that while the variability between the individually matched observations is large, the precision of rigorously simultaneous time series means is quite good and allows meaningful comparison. In other words, finding the mean of rigorously simultaneous reflectivity observations filters out the variability due to both instrument error and the natural variation of precipitation fields sufficiently that calibrations are possible.

This paper is organized as follows. The disdrometer, profiling radars, and scanning radar datasets are introduced in section 2. The profiling radar measurement error is determined in section 3. The profiling radar reflectivity is absolutely calibrated using the surface disdrometer observations in section 4. Sections 5 and 6 develop the methodology for using the profiler to calibrate and monitor the scanning radar reflectivity. The discussion of results and conclusions is in section 7.

2. Datasets

This paper presents observations from four different instruments: one surface disdrometer, two vertically pointing profiling radars, and one WSR-88D scanning radar.

a. Disdrometer observations

The observations from a model RD-69 surface disdrometer manufactured by Distromet, Inc. (Switzerland), recorded the precipitation reaching the surface. This disdrometer is also commonly known as the Joss–Waldvogel disdrometer in honor of its inventors (Joss and Waldvogel 1969). The disdrometer essentially measures the momentum of the raindrops hitting the 50-cm^2 sensor head and converts these individual impacts into raindrop diameter estimates from 0.3 to 5.3 mm in 127 nonuniform size intervals [see Sheppard and Joe (1994) and the work referenced in that study for more details about the disdrometer operation]. The counts in the raindrop diameter size bins are accumulated over 1-min intervals to yield minute-by-minute DSDs, which are converted into estimates of the surface precipitation radar reflectivity.

b. Profiler observations

Two vertically pointing profiling radars were deployed by the National Oceanic and Atmospheric Administration (NOAA) Aeronomy Laboratory in support of TEFLUN-B. One operated at 915 MHz and the other at 2835 MHz. The two stationary, dish antennas were placed next to each other, and the observations were synchronized to ensure that the two radar systems were observing approximately the same atmospheric volumes at the same time. Both radar systems had 5° beamwidths and had the same vertical (105 m) and temporal resolution (60 s). Figure 1 shows a photograph of the surface disdrometers and profiling radars during the TEFLUN-B campaign, and Table 1 lists the system parameters.

c. Scanning weather radar observations

The NWS operates a WSR-88D radar (KMLB) near Melbourne, Florida, which is on the east coast of Florida and south of Cape Canaveral. The KMLB reflectivity used in this study was extracted from the Level II Archive WSR-88D radar data publicly accessible via the NOAA National Climatic Data Center (NCDC) archive (www.ncdc.noaa.gov). Descriptions of the WSR-88D radar operating conditions and NEXRAD operations can be found in Crum et al. (1993), Crum and Alberty (1993), and Crum et al. (1998). The operational Level II Archive data product consists of reflectivity, mean radial Doppler velocity, and spectral width at each measurement cell defined by the coordinates of time, range gate, azimuth angle, and elevation angle. These data were screened to extract only the closest observation directly over the profiler site for each elevation angle without any interpolation. Table 2 lists the scanning radar system operating parameters.

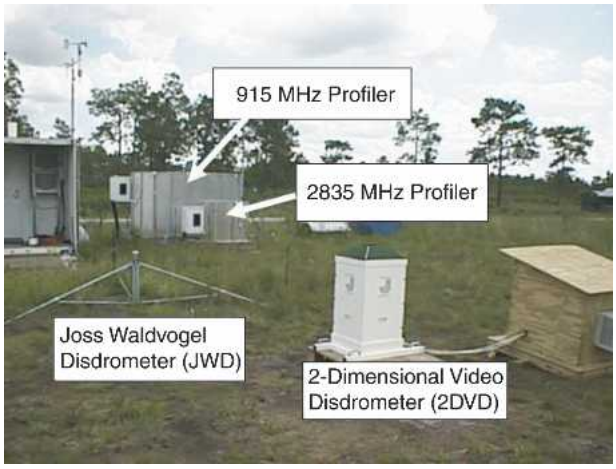

FIG. 1. Photograph of the surface disdrometers and profiling radars located at the Triple-N Ranch 36 km west of the Melbourne, FL, WSR-88D radar (KMLB).

3. Uncertainties in profiler reflectivity estimates

It is very difficult to determine the error characteristics of instruments that measure precipitation parameters. This difficulty is largely due to the variability of precipitation in space and time. To quantify the pre-

TABLE 1. Profiler operating parameters during the TEFLUN-B field campaign.

Parameters	915-MHz profiler	2835-MHz profiler
Wavelength	32.8 cm	10.6 cm
Peak power	500 W	5 W
Antenna	3-m shrouded dish	1.2-m shrouded dish
Beamwidth	5°	5°
Height resolution	105 and 255 m	105 and 255 m
Max height sampled	18.0 km	18.0 km
Max radial velocity	± 20 m s^{-1}	± 20 m s^{-1}
Approximate sensitivity at 1 km	0–62 dBZ	0–62 dBZ
Spectral points	256	256
Dwell time	30 s	30 s
Pulse repetition rate	10 000 Hz	10 000 Hz

TABLE 2. NEXRAD scanning radar operating parameters during volume scan mode (VCP 11).

Parameters	WSR-88D
Peak power	750 kW
Beamwidth	0.95°
Unambiguous range	460 km
No. of range gates	460
Range gate spacing	1 km
Azimuthal spacing	~1°
Rotation rate	~19° s^{-1}
Pulse repetition rate	325 Hz
No. of linear samples	64
Reflectivity resolution	0.5 dBZ
Temporal resolution	~5 min

cipitation error characteristics for improved QPE, it is informative to break the error characteristics down into factors related to the instrument technology and factors related to the precipitation processes. If Z_{observed} and Z_{true} represent the observed and true reflectivity, the error characteristics can be written as (Bringi and Chandrasekar 2001)

$$Z_{\text{observed}} = Z_{\text{true}} + \varepsilon_{\text{measurement error}} + \varepsilon_{\text{representativeness error}}. \quad (1)$$

The error characteristics can be quantified using the variance statistic

$$\text{var}(Z_{\text{observation}} - Z_{\text{true}}) = \sigma^2_{\text{measurement error}} + \sigma^2_{\text{representativeness error}}. \quad (2)$$

The representativeness error represents the precipitation spatiotemporal variation. It is very difficult to quantify the representativeness error because discretely sampling moving precipitation systems scales the horizontal structure of the precipitation (Fabry 1996). More work is needed to quantify and understand this error for QPE purposes.

The measurement error quantifies the limitations of the instrument and is more tractable. Here we quantify it by observing the same volume of precipitation with two similar radars. The two instruments have the same sampling volumes and dwell times so that the representativeness error is nearly identical for both instruments. The observed variance of the reflectivity differences is used to quantify the measurement error.

The 915- and 2835-MHz vertically pointing profiling radars were configured to observe the same atmospheric volumes with the same temporal resolution. Figure 2 shows the reflectivity difference between the 2835- and 915-MHz profiler observations for all 105-m resolution observations between 0.5 and 4.0 km during the TEFLUN-B campaign. To ensure that only precipitation observations were analyzed, all used observations had reflectivities greater than 10 dBZ and downward velocities greater than 4 m s^{-1}. These two constraints limit the radar dataset to 74 585 observations and ensure that both radars are identifying the Rayleigh scattering component of the Doppler spectrum [See the work of Ralph (1995) and Williams et al. (2000) to identify hydrometeors in profiler observations.]

The statistical bias, standard deviation, and 95% confidence interval for the profiler reflectivities were estimated using

$$B = \frac{1}{n}\sum_n (Z_{2835\text{ MHz}} - Z_{915\text{ MHz}}), \quad (3)$$

$$\sigma = \left\{\frac{1}{n}\sum_n [(Z_{2835\text{ MHz}} - Z_{915\text{ MHz}})^2] - B^2\right\}^{1/2}, \quad (4)$$

and

$$L_{95\%} = \pm t_{95\%}\frac{\sigma}{\sqrt{n}}, \quad (5)$$

where n is the number of samples, $Z_{2835\text{ MHz}}$ and $Z_{915\text{ MHz}}$ are the observed reflectivities from both profilers, and $t_{95\%}$ is the 95th percentile of the t distribution with n degrees of freedom (Anagnostou et al. 2001). Figure 2c shows the probability distribution function (PDF) of the 915-MHz reflectivity expressed in dBZ units [10log(mm^6 m^{-3})]. Figure 2a shows the PDF of the reflectivity difference (2835 − 915 MHz). The shape of the PDF is important for interpreting the statistical calculations between the two datasets. The near-Gaussian-shaped PDFs indicate that the datasets are nearly normally distributed. The standard deviation and 95% confidence interval estimates have statistical significance only when the datasets are normally distributed. Since the observed reflectivity PDFs expressed in linear units (mm^6 m^{-3}) were not normally distributed (not shown), all statistical calculations in this study were performed with the reflectivity in dBZ units.

The total bias in reflectivity between the two profiling radars was zero because both profilers were absolutely calibrated using the surface disdrometer. Section 4 describes this calibration. The standard deviation of the reflectivity difference was 0.57 dBZ and is shown with straight lines in Fig. 2a. The 95% confidence interval about the mean difference for these 74 585 observations was 0.0034 dBZ. For each 1-dBZ interval of 915-MHz reflectivity the bias and 95% confidence in-

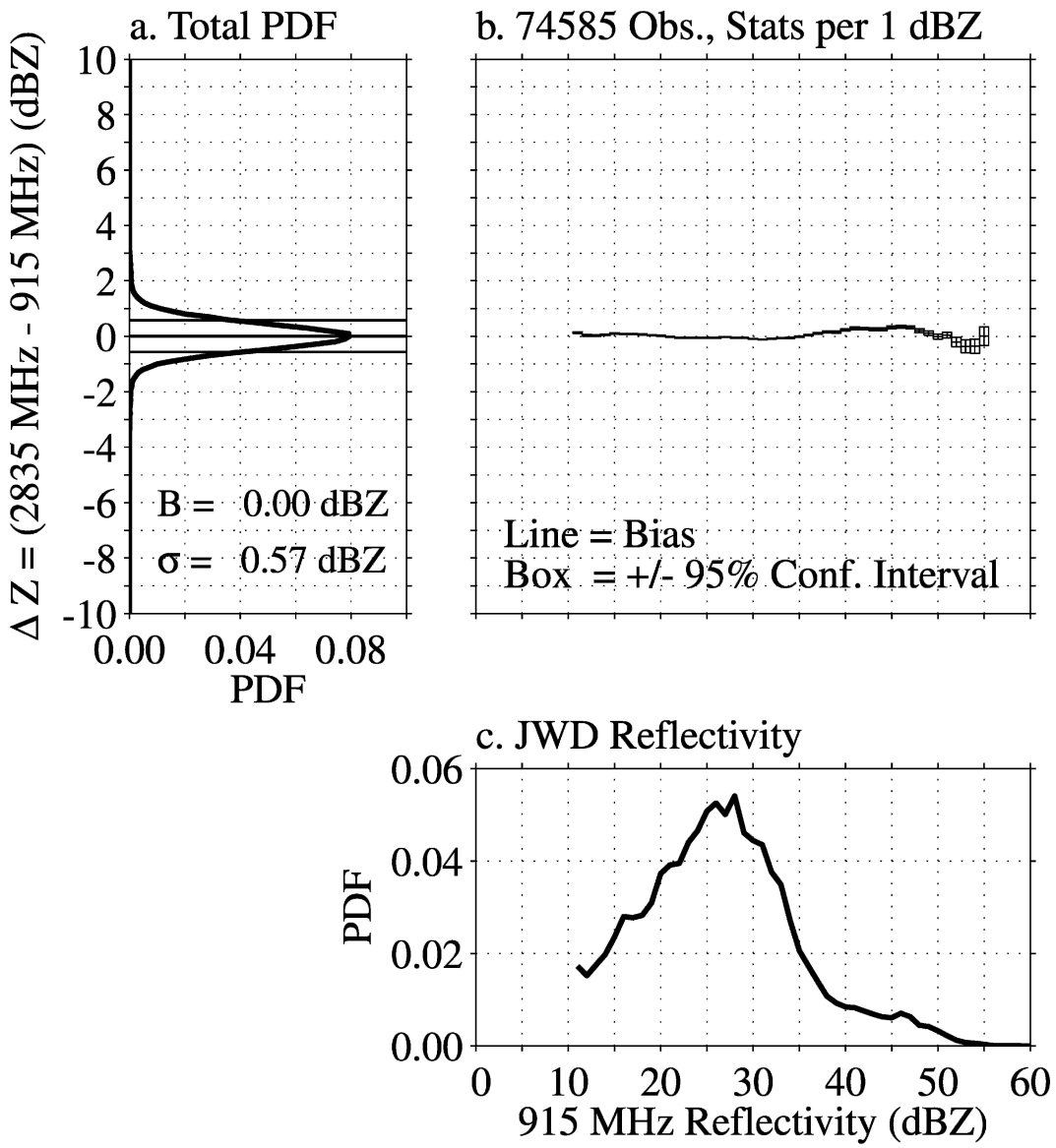

FIG. 2. Reflectivity difference (2835 − 915 MHz) between the two vertically pointing profiling radars using the 74 585 simultaneous observations over the 21 range gates between 0.5 and 4.0 km. (a) The total PDF for all difference observations as well as the bias and the bias plus/minus the standard deviation ($B \pm \sigma$). (b) A box symbol vs each 1-dBZ interval of 915-MHz profiler reflectivity. The bias of each 1-dBZ interval is shown with a horizontal line, and the box indicates the bias plus/minus the 95% confidence interval ($B \pm L_{95\%}$). (c) The PDF of the 915-MHz profiler reflectivity.

terval were calculated and are shown with box symbols in Fig. 2b.

This analysis provides a quantitative estimate of the measurement error of both profilers. Assuming that both profilers have the same error characteristics, the measurement error variance for either profiler is estimated to be 0.16 dBZ^2. This is calculated from $\text{var}(Z_{2835\text{ MHz}} - Z_{915\text{ MHz}}) = 0.57^2 = 2\sigma^2_{\text{measurement error}}$. Quantifying the measurement error has two implications. First, the measurement error of an individual reflectivity estimate can be quantified using the standard deviation statistic. For these profilers, for example, the uncertainty of an individual reflectivity estimate can be quantified as $Z_{\text{observed}} \pm \sigma_{\text{measurement error}}$, or ±0.4 dB$Z$. And second, as is shown later in this paper, the observed variance of reflectivity differences between a profiler and a disdrometer and between a profiler and a scanning radar were much larger than $\sigma^2_{\text{measurement error}}$,

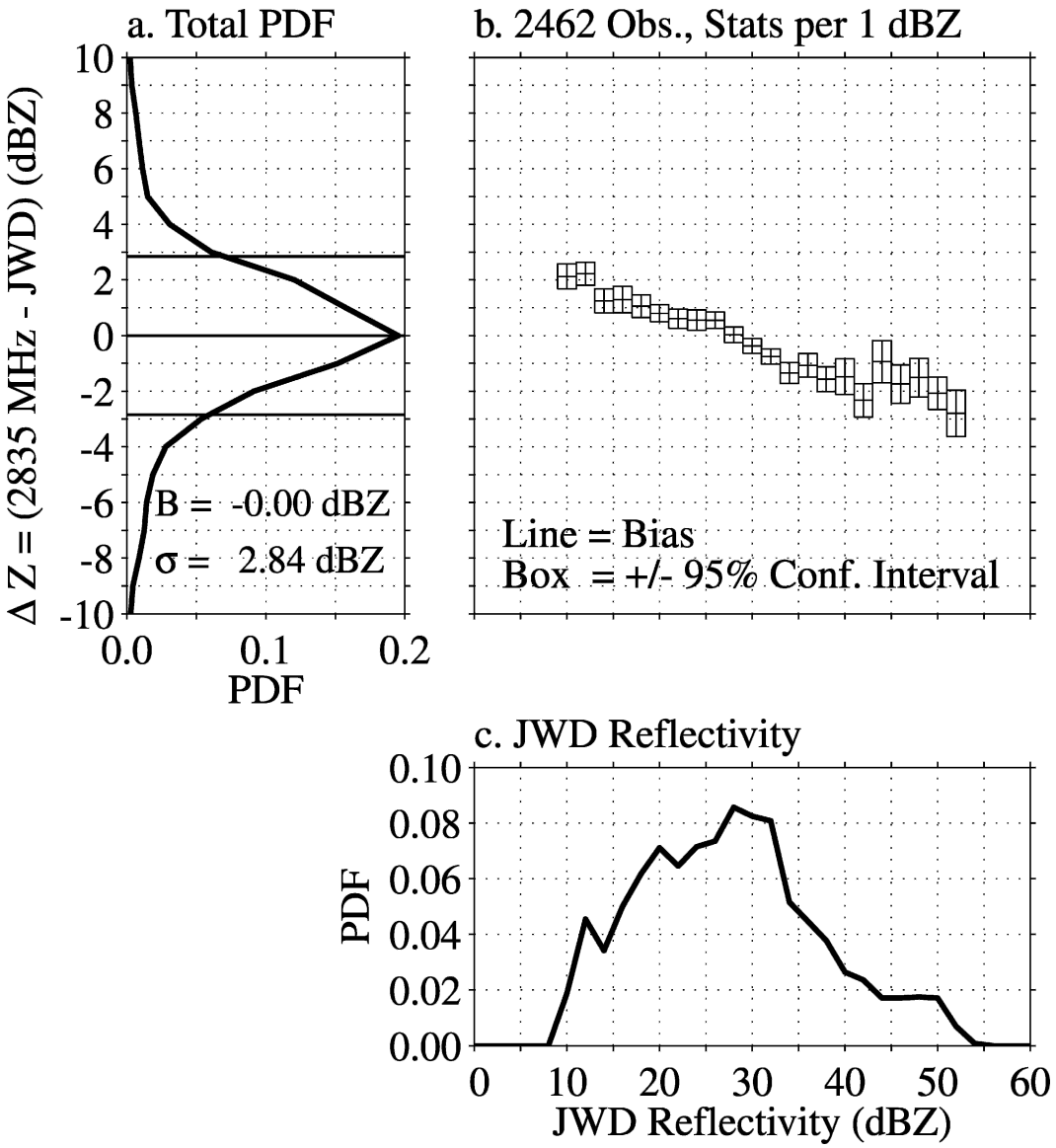

FIG. 3. Same as in Fig. 2, but for the reflectivity difference (2835 MHz − disdrometer) between the 2835-MHz profiler and surface disdrometer using the 2462 simultaneous minute observations. The selected profiler pulse volume is centered 308 m above the ground.

verifying the contribution of the representativeness error.

4. Profiler calibration using disdrometer observations

The profilers were absolutely calibrated using the surface disdrometer. While the surface disdrometer measured the raindrops impacting the sensor head, the lowest 105-m radar pulse volume was centered 308 m above the ground. The mismatch in volume size and the displacement of the two sample volumes add to the reflectivity difference variance between the two measurements. To ensure that both instruments were simultaneously observing rain, the observations were screened to require that the profiler had reflectivities greater than 10 dBZ and mean downward Doppler velocities greater than 4 m s^{-1}, while the surface disdrometer was required to have observed at least 25 raindrops in the minute sample. The reflectivity differences between the simultaneous minutes of the 2835-MHz profiler and surface disdrometer observations are shown in Fig. 3 using the format introduced in Fig. 2.

The PDF of profiler minus disdrometer reflectivity

difference is shown in the left-hand panel of Fig. 3. The profiler reflectivity was calibrated so that the mean reflectivity difference was zero. The standard deviation of the reflectivity difference of 2.84 dBZ (shown as straight lines in Fig. 3a) is much larger than the profiler-to-profiler reflectivity difference standard deviation of 0.57 dBZ estimated in section 3. The increased reflectivity difference variance is due to the different technologies of the two instruments, the different sampling volumes, and the physical separation of the two sampling volumes. The only consequence, however, is that a somewhat larger number of observations are needed to achieve a desired standard error of the mean.

In examining Fig. 3b, it is interesting to note that the bias of the reflectivity difference varies as a function of the JWD reflectivity. The reflectivity difference becomes more negative as the JWD reflectivities increase. While the bias varies with JWD reflectivity, the 95% confidence intervals are insensitive to the JWD reflectivity below 40 dBZ. The bias variation is curious and indicates an unaccounted effect in either the profiler or disdrometer observations. The cause is uncertain. One possibility is that near the surface, convective rains with large reflectivities are also associated with downdrafts due to evaporative cooling (Srivastava 1987). Thus, while the air motion is zero at the surface, the raindrops in a downdraft would be falling faster than their terminal velocities when they impacted the disdrometer sensor. This would cause the disdrometer to overestimate both the raindrop size and the reflectivity. More analysis is needed to validate this hypothesis and to understand the trend in the bias.

5. Calibrating the scanning weather radar

Before the calibrated profiling radar can be used to calibrate and monitor the scanning radar reflectivity, the difference in spatial and temporal sampling of the two instruments needs to be reconciled. The scanning radar observations have larger radar pulse volumes and longer gaps of time between samples than the profiling radars. Even after the profiling radar observations are averaged in altitude to approximate the vertical extent of the scanning radar pulse, and after the radars are matched in time and height, there is still considerable mismatch between the two sampling volumes that will contribute to the calculated reflectivity difference variance.

a. Differences in sampling volumes: Temporal and spatial

During the TEFLUN-B campaign, the KMLB radar sequentially swept through all azimuth angles in approximately 1° increments at 14 elevation angles from 0.5° to 19° above the horizon until a complete volume scan was obtained. During the 5 min required to complete one volume scan, the radar antenna was constantly rotating at a rate of approximately 19° s^{-1}. Thus, the radar dwelled over the profiler for only a fraction of a second during each elevation scan. A WSR-88D radar vertical profile of observations over the profiler site consists of a short dwell time (approximately 50 ms) at each elevation angle, followed 20 s later (after the WSR-88D scans 360° in azimuth) by an observation at the next higher elevation angle. The dwell at any particular elevation is repeated once every 5 min.

For each scanning radar observation over the profiler site, six profiler range gates are averaged to match the vertical extent of the scanning radar observation. At a range of 36 km, the vertical extent of the 0.95° WSR-88D radar beam is 630 m when rounded to a multiple of the profiling radar pulse length of 105 m. The 1-km-long scanning radar pulse length (constructed from averaging four 250-m consecutive radar pulses) implies that the WSR-88D radar sample volume is of the order 3×10^8 m^3, which is three orders of magnitude larger than a single profiler sampling volume.

b. Simultaneous profiler and scanning radar observations

During the months of August and September 1998, the surface disdrometer, vertically pointing profilers, and scanning radar were in continuous operation. Figure 4 shows an example of the vertical and temporal resolution of the observed reflectivity over the profiler by the vertically pointing 2835-MHz profiling radar and by the Melbourne WSR-88D radar. Figure 4a shows the profiler reflectivity at the original 105-m vertical and 1-min temporal resolution. The 30 original profiler observations (5 in time and 6 in range) that matched the 5-min time and 630-m altitude resolution of the WSR-88D radar measurement cell were averaged in linear units and are shown in dBZ units in Fig. 4b. The variation of reflectivity within the WSR-88D radar measurement cell is quantified by estimating the standard deviation of the 30 original profiler observations expressed in log units, $\sigma_{5\text{min},630\text{m}}$, and is shown in Fig. 4d. The Melbourne WSR-88D radar reflectivities for this rain event are shown in Fig. 4c.

Even with the 630-m vertical resolution, the time–height displays of reflectivity from the profiler and scanning radar can be used to diagnose precipitation regimes fairly well. The large reflectivities at low altitudes and the extension of reflectivities to high altitudes (~10 km) near 0530 UTC are indicators of convective rain. The stratiform rain is identified by the radar bright

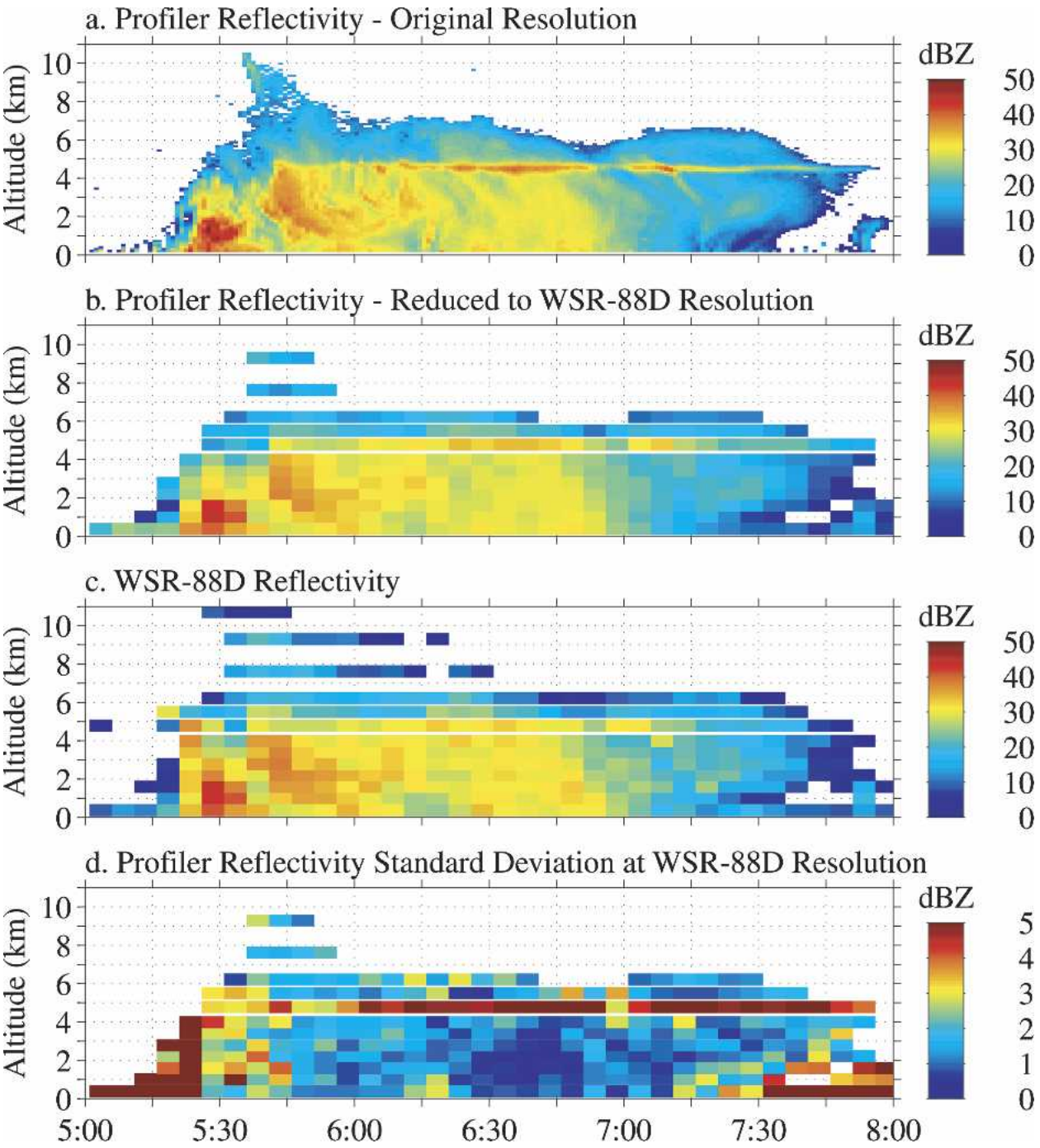

FIG. 4. Time–altitude cross sections of profiling and scanning radar observations during a rain event passing over the profiler site on 21 Aug 1998. (a) The profiler reflectivity in the original 1-min temporal and 105-m vertical resolution. (b) The profiler reflectivity after being averaged to the 5-min temporal and 630-m vertical resolution of the WSR-88D radar resolution over the profiler site (averaged in linear units and plotted in log units). (c) The WSR-88D reflectivity at the original 5-min temporal and 630-m vertical resolution over the profiler site. (d) The profiler reflectivity standard deviation, $\sigma_{5\text{min},630\text{m}}$, calculated for each 5-min and 630-m resolution (calculated in log units).

band that is well defined in the 105-m profiler observations but not so well distinguished in the 630-m observations from 0630 to 0730 UTC.

While Fig. 4 shows the time–altitude comparison between the profiler and scanning radar reflectivity, Fig. 5 shows reflectivity profiles obtained during two different volume scans. A convective (stratiform) profile at 0531 (0636) UTC in Fig. 5a (Fig. 5b) shows the scanning

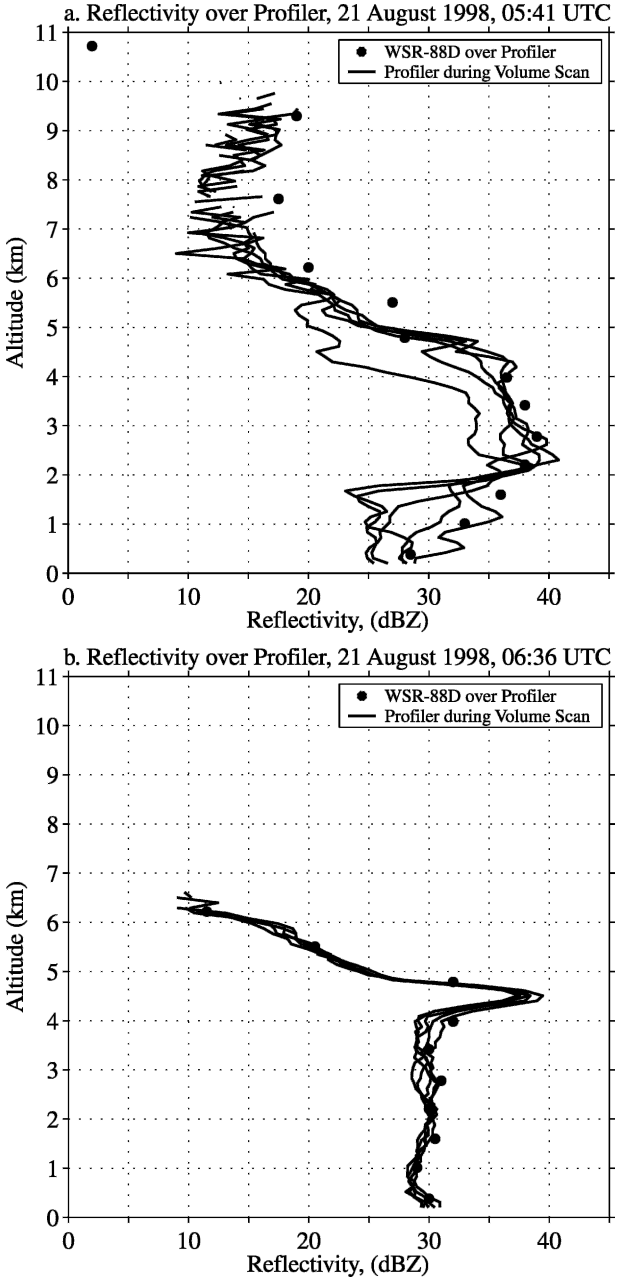

FIG. 5. Profiles of reflectivity from the profiling and scanning radars during two 5-min volume scans representing two different rain regimes during the 21 Aug 1998 rain event. (a) The reflectivity profile during the convective portion of the storm at 0541 UTC. The scanning radar observations are shown with filled circles and the five 1-min profiler observations are shown with thin lines. (b) The reflectivity profile during the stratiform portion of the storm at 0636 UTC. The coarse vertical resolution of the scanning radar does not resolve the radar bright band near 4.5-km altitude.

radar reflectivity with filled circles and the five 1-min profiler reflectivity profiles with thin lines. The convective rain profile (Fig. 5a) has more variation in profiler reflectivity than the stratiform rain profile (Fig. 5b) and has reflectivities greater than 10 dBZ extending above 9 km in altitude. The stratiform rain profile has a well-defined radar bright band resolved by the profiling radar but is not resolved by the scanning radar because of the unique combination of tilt angles and range from the scanning radar. The bright band is resolved by the scanning radar in other precipitation events when the bright band is at a lower altitude.

The increased reflectivity variance for the convective rain profile compared with the stratiform rain profile is consistent with our understanding of the natural variations in the precipitation processes (see Houze 1993). Obviously, then, the best comparisons between two instruments that have close but different sampling volumes would occur in stratiform situations, when the precipitation processes have the least amount of spatiotemporal variation. The profiler reflectivity standard deviation, $\sigma_{5\text{min},630\text{m}}$, over each 5-min and 630-m time–altitude window that corresponds with the WSR-88D radar resolution quantifies the temporal and vertical variation of the reflectivity. Indeed, the $\sigma_{5\text{min},630\text{m}}$ is a fair indicator of precipitation regime. For example, it is larger during the convective region of the storm (0515–0545 UTC) and smaller during the stratiform regime (0600–0715 UTC). Note, however, that $\sigma_{5\text{min},630\text{m}}$ increases near the end of the event from 0730 to 0745 UTC due to gradients near the edges of the storm. In these observations, the radar bright band is clearly identified by large $\sigma_{5\text{min},630\text{m}}$ values due to the change in reflectivity over the 630-m vertical altitude used in calculating $\sigma_{5\text{min},630\text{m}}$.

c. *Profiling and scanning radar reflectivity differences—21 August 1998 case study*

The Melbourne WSR-88D radar reflectivities are tested for bias using the calibrated profiler reflectivities from the one rain event of 21 August 1998 shown in Fig. 4. Using only the six lowest tilt angles that correspond to altitudes between 0.4 and 3.4 km to avoid the altitudes that include the melting layer, 179 individual profiler and scanning radar reflectivity differences were obtained and are shown in Fig. 6 versus profiler reflectivity and versus $\sigma_{5\text{min},630\text{m}}$.

For this single rain event, the observed reflectivity bias between the two radars is 0.44 dBZ, the standard deviation is 2.58 dBZ, and the 95% confidence interval is 0.32 dBZ. Thus, while the calculations indicate large variability in individual profiler to scanning radar comparisons, the precision of the series is good. These calculations are consistent with other profiling to scanning radar comparisons (May et al. 2002). The profiler reflectivity PDF shown in Fig. 6c indicates a peak number of observations with reflectivities near 30 dBZ. The

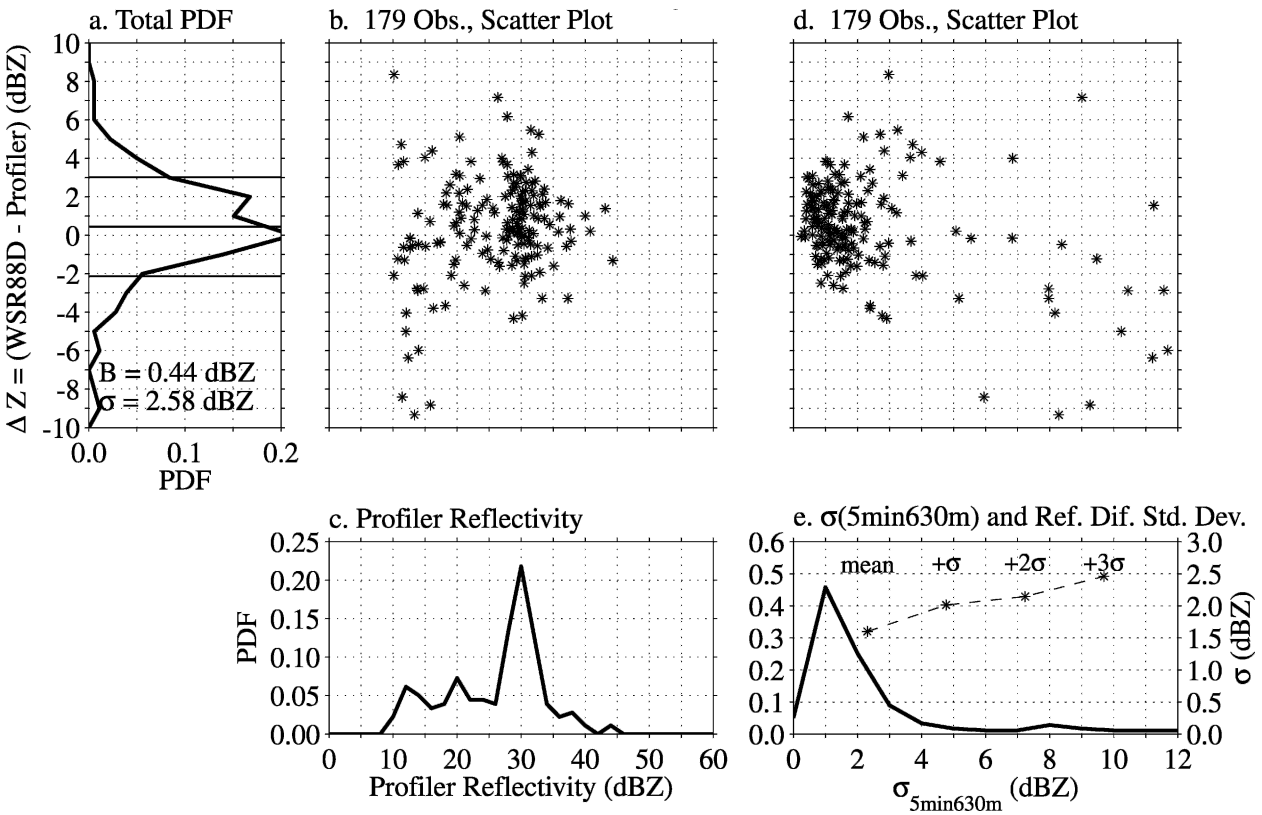

FIG. 6. Difference in scanning radar and profiling radar reflectivity (WSR-88D − profiler) for the 21 Aug 1998 rain event shown as a function of profiler reflectivity and profiler reflectivity standard deviation, $\sigma_{5\text{min},630\text{m}}$, which represents the variance over a scan. The 179 simultaneous observations from the lowest six tilt angles are used (0.4–3.4 km) to avoid the observations contaminated by the radar bright band. (a) The PDF of the reflectivity difference. Also shown are the PDFs for the (c) profiler reflectivity and (e) profiler reflectivity standard deviation, $\sigma_{5\text{min},630\text{m}}$; and scatterplots of the reflectivity difference as a function of (b) profiler reflectivity and (d) profiler reflectivity standard deviation, $\sigma_{5\text{min},630\text{m}}$. The reflectivity difference standard deviation is estimated for observations selected by use of four different $\sigma_{5\text{min},630\text{m}}$ thresholds, and the results are shown with a dashed line referenced to the scale on the right-hand side of (e).

spread in the reflectivity difference near 30 dBZ is approximately plus and minus the standard deviation while there is more variation in reflectivity difference at smaller reflectivities. Figure 6d shows the observed reflectivity differences as a function of $\sigma_{5\text{min},630\text{m}}$, and Fig. 6e shows the PDF of $\sigma_{5\text{min},630\text{m}}$. Note that the spread in the reflectivity difference is greater for $\sigma_{5\text{min},630\text{m}} \sim 2$ dBZ, suggesting that $\sigma_{5\text{min},630\text{m}}$ can be used to identify observations with smaller reflectivity variance.

To explore the variability quantitatively, four different thresholds of $\sigma_{5\text{min},630\text{m}}$ are determined from the mean plus multiples of the standard deviation of $\sigma_{5\text{min},630\text{m}}$ [e.g., $\overline{\sigma_{5\text{min},630m}} + n\ \text{std}(\sigma_{5\text{min},630m})$, where n = 0, 1, 2, 3]. For each threshold, all observations associated with $\sigma_{5\text{min},630\text{m}}$ less than the threshold are used to estimate the rain event reflectivity difference standard deviation, and the results are plotted with the dashed line using the right-hand axis in Fig. 6e. While the method of estimating the threshold could be refined, this simple threshold still provides an objective method of removing outliers from the rain event population based on a physical measurement.

d. Profiling and scanning radar reflectivity differences—2 months of observations

During the 2-month period of the TEFLUN-B experiment, 21 rain events passed over the profiler site and were observed by the surface disdrometer, profiling radars, and the Melbourne WSR-88D radar. These 21 rain events are summarized in Table 3, which indicates the storm duration and the statistics of simultaneously matched profiling and scanning radar observations. Section 5c shows that large values of the $\sigma_{5\text{min},630\text{m}}$ statistic are associated with outliers. Therefore, all of the rain events were screened to remove all observations with $\sigma_{5\text{min},630\text{m}}$ greater than the mean plus one standard deviation of $\sigma_{5\text{min},630\text{m}}$. Although this screening only removes about 10% of the observations

TABLE 3. Statistics for each rain event using the lowest six tilt angles. The columns include date, hour, number of observations (no. obs), mean plus standard deviation of $\sigma_{5\text{min},630\text{m}}$ (threshold), reflectivity bias (bias), reflectivity difference standard deviation (σ), and 95% confidence interval (95% C.I.). The asterisk (*) denotes the rain events used in the statistics of the 14 selected rain events.

Date	Hour (UTC)	No. obs	Threshold	Bias	σ	95% C.I.
10 Aug 1998	1900–2100	38	11.90	−0.53	4.65	1.28
13 Aug 1998	0200–0500	67	7.41	2.34	3.14	0.64
15 Aug 1998	2000–2400	48	7.85	−2.69	3.28	0.79
16 Aug 1998	2000–2100	33	12.57	−1.66	4.24	1.25
20 Aug 1998	1400–1900	85	5.11*	0.95	2.55	0.46
21 Aug 1998	0500–1000	159	4.77*	0.82	2.01	0.26
21 Aug 1998	1400–1700	105	5.19*	1.39	2.31	0.37
22 Aug 1998	0000–0700	223	5.15*	0.65	2.41	0.27
2 Sep 1998	1800–2400	59	7.90	−1.43	3.80	0.83
3 Sep 1998	1600–2300	70	11.55	−1.00	4.22	0.84
6 Sep 1998	1900–2400	61	3.38*	0.54	2.08	0.45
7 Sep 1998	1800–2400	142	4.57*	0.56	3.64	0.51
8 Sep 1998	2100–2400	59	5.33*	0.19	3.04	0.66
9 Sep 1998	2200–2400	20	5.82	−0.22	2.95	1.13
17 Sep 1998	1800–2400	259	3.02*	0.29	2.32	0.24
18 Sep 1998	0000–0300	47	5.80*	0.01	2.35	0.57
19 Sep 1998	0200–0900	279	2.34*	0.91	1.62	0.16
19 Sep 1998	1700–2300	238	3.18*	0.62	1.91	0.20
20 Sep 1998	1500–2000	145	4.91*	0.60	2.28	0.32
21 Sep 1998	1900–2300	118	4.46*	0.40	2.51	0.38
22 Sep 1998	1900–2300	142	4.67*	0.85	2.31	0.32
All 21 rain events		2397	—	0.48	2.71	0.09
14 rain events*		2062	—	0.66	2.36	0.09

in each rain event, it successfully removes the largest outliers. The thresholds for each rain event are also listed in Table 3.

The statistics from all 21 rain events are listed near the bottom of Table 3 and are shown in Fig. 7 using the multipanel format introduced in Fig. 6. The reflectivity difference PDF plotted in Fig. 7a shows that the distribution is slightly asymmetric with a bias value of 0.48 dBZ. The reflectivity difference statistics are shown as a function of every 2-dBZ interval of profiler reflectivity in Fig. 7b using the box symbols defined in Figs. 2 and 3. Note that the bias appears independent of profiler reflectivity until about 40 dBZ. After 40 dBZ, the number of observations decreases substantially and the observations are predominately from convective situations, suggesting that the time–volume mismatch is playing an important role.

The reflectivity difference plotted as a function of $\sigma_{5\text{min},630\text{m}}$ in Fig. 7d clearly shows the tendency of the spread to increase as the convective situation becomes more variable. It also shows a tendency for the WSR-88D profiler bias to become more negative as $\sigma_{5\text{min},630\text{m}}$ increases. This tendency may or may not be real, as the number of observations for large $\sigma_{5\text{min},630\text{m}}$ is quite small (see Fig. 7e).

Figures 7d and 7e show that as $\sigma_{5\text{min},630\text{m}}$ increases, the 95% confidence interval broadens and the bias becomes more negative. While each storm has been filtered by the storm $\sigma_{5\text{min},630\text{m}}$ threshold, the thresholds listed in Table 3 indicate that some storms are more variable than others. By examining each rain event it was determined that the events with large $\sigma_{5\text{min},630\text{m}}$ thresholds were convective events that contained short-duration (on the order of 30 min or less) convective cells. Seven of these convective rain events were subjectively screened out, and the remaining 14 rain events were combined to produce the ensemble statistics listed in Table 3 and shown in Fig. 8. Since the largest $\sigma_{5\text{min},630\text{m}}$ threshold of the selected 14 rain events is 5.80, the horizontal axis of Figs. 8d and 8e only extends to 6 dBZ. The reflectivity difference bias, 95% confidence interval of the bias, and the standard deviation for the 14-rain-event dataset are 0.66, 0.09, and 2.36 dB, respectively.

6. Monitoring the scanning radar reflectivity calibration

The analysis presented in section 5 shows how the profiler and scanning radar reflectivities can be combined to calibrate the scanning radar. This calibration procedure can be performed for each rain event (as described in section 5c), or the individual rain events can be combined to produce an ensemble of observa-

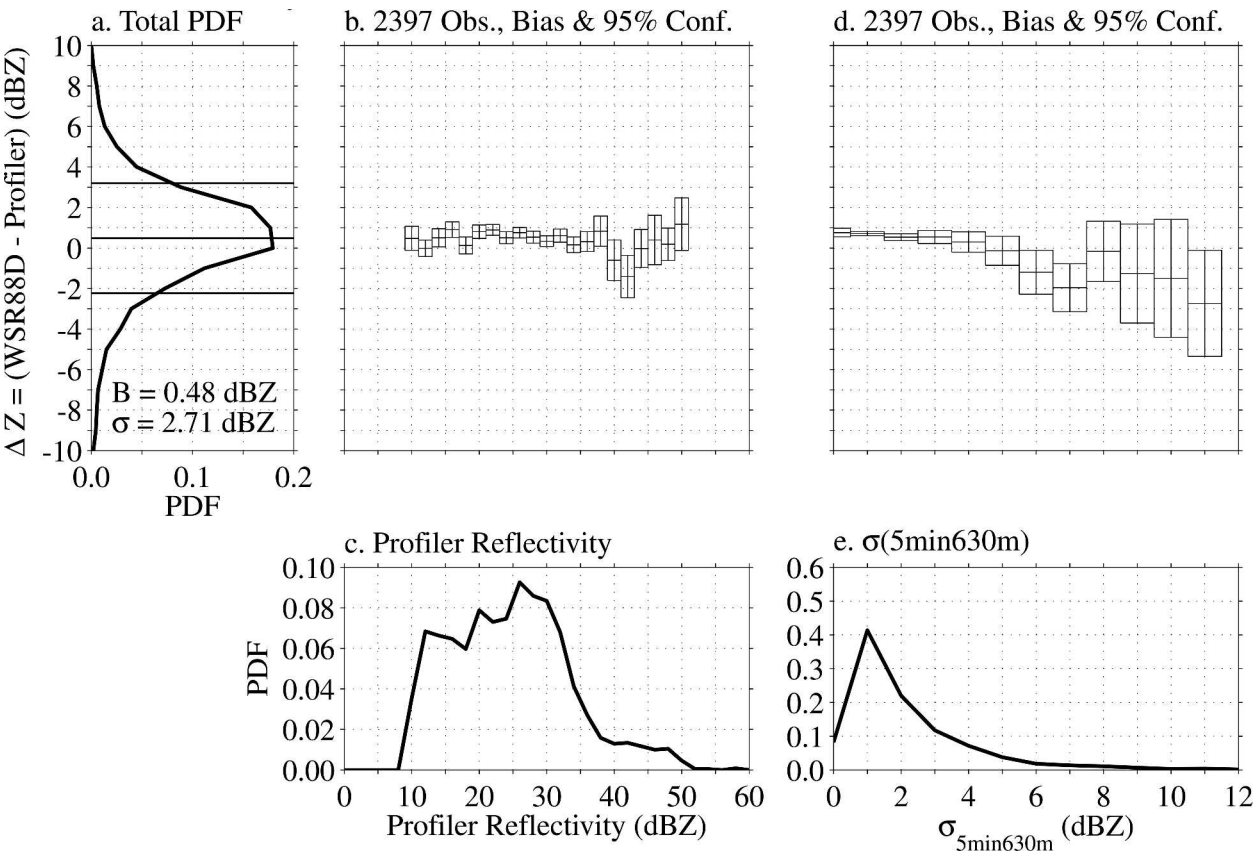

FIG. 7. Same as Fig. 6 except for all observations from the 21 rain events during the 2-month campaign. The observations are tabulated in Table 3 and have been selected using $\sigma_{5\text{min},630\text{m}}$ as discussed in the text. The box symbols in (b) and (d) indicate the bias and the 95% confidence intervals of the 2397 observations.

tions (as described in section 5d). Deviations in the storm-to-storm statistics from the ensemble statistics or trends in the storm-to-storm statistics may indicate that the performance of the scanning or profiling radar is changing with time. If this change in performance is detected by the scanning radar personnel, then they could take appropriate actions in interpreting the precipitation products. Also, they can contact the engineering staff, who would determine the cause of the problem and make the necessary corrections. The benefit of this instrument monitoring methodology is that the WSR-88D radar performance can be tracked from storm to storm. This will provide more information to the radar operators and the confidence that the radar is operating correctly between the periodically scheduled maintenance.

The storm bias and 95% confidence interval for the 21 rain events simultaneously sampled by the profiling and scanning radars are shown in Fig. 9a. The ensemble bias and 95% confidence interval is shown on the right-hand side of Fig. 9a with the total bias shown as a straight line throughout the 2-month period. The bias and 95% confidence interval statistics are shown in Fig. 9b for the 14 rain events that are used to generate the ensemble statistics shown in Fig. 8. The seven rain events identified as having large $\sigma_{5\text{min},630\text{m}}$ thresholds are also the outlier storms shown in Fig. 9a. No trend was evident in the storm-to-storm statistics or a sudden change in the storm statistics. This indicates that both the scanning and profiling radars were stable throughout this 2-month campaign.

7. Discussion

It is very difficult to quantify the uncertainties of precipitation estimates because of the variability of the precipitation in time and space. These uncertainties can be described as instrumental measurement error and as representativeness error. The measurement error is associated with the precision of the instrument, and the representativeness error is associated with incomplete sampling of the variable precipitation field. In this paper we present the measurement error from profiling radars using two vertically pointing profiling radars to

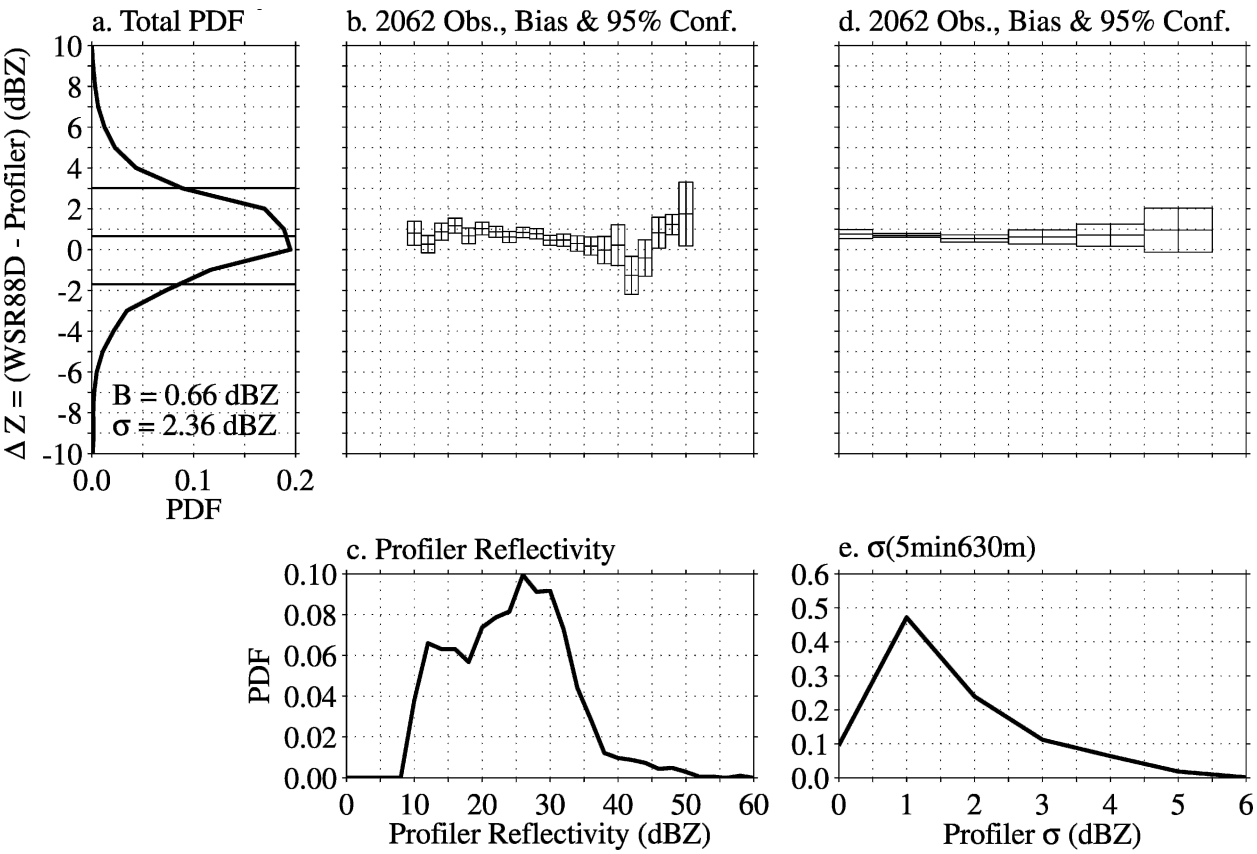

FIG. 8. Same as Fig. 7 except for the observations from the 14 selected rain events during the 2-month campaign. The selected rain events are indicated in Table 3.

observe the same volume of the atmosphere. As was demonstrated in Gage et al. (2004), this methodology enables us to quantify the measurement error in a variable precipitation field. Using 74 585 simultaneous precipitation observations, the reflectivity difference standard deviation was 0.57 dB*Z*, resulting in a single observation precision of 0.4 dB*Z*. These results are consistent with the estimated measurement error for profilers used in TEFLUN-B (Gage et al. 2004) and with the estimated error of less than 0.5 dB*Z* reported by May et al. (2001) using a well-calibrated C-band polarimetric research radar to calibrate a 920-MHz profiler. The 95% confidence interval of the bias was 0.0034 dB*Z* for the 74 585 observations.

During the TEFUN-B campaign, a surface disdrometer was used to absolutely calibrate the vertically pointing profiling radar. There were 2462 simultaneous profiler and disdrometer observations during this 2-month campaign. The reflectivity difference standard deviation of 2.84 dB*Z* was substantially larger than the standard deviation between two profilers. This is partly due to the different sampling volume sizes and the 308-m separation between the two sampling volumes. Another factor is that the precision of a 1-min disdrometer observation is on the order of 2 dB*Z* (Gage et al. 2004). The large number of simultaneous observations enables the 95% confidence interval about the bias to be ±0.09 dB*Z*.

After the profiler was absolutely calibrated by the surface disdrometer, the profiler reflectivity was used as a transfer standard and compared with the simultaneous WSR-88D radar reflectivity measurements made over the profiler site. Since the scanning radar required 5 min to complete a volume scan and the vertical extent of the radar beam over the profiler was 630 m, the 1-min and 105-m vertical resolution profiler observations were averaged to match the WSR-88D radar resolution. A novel feature of this study was that the reflectivity variation during the 5-min and 630-m resolution window was quantified using the standard deviation of the profiler reflectivity, $\sigma_{5\text{min},630\text{m}}$. The direct correlation of $\sigma_{5\text{min},630\text{m}}$ with the reflectivity difference variance led to the $\sigma_{5\text{min},630\text{m}}$ statistic being used to detect and remove outliers associated with convective rain.

During the 2-month TEFLUN-B campaign, there were 21 rain events that had disdrometer, profiler, and

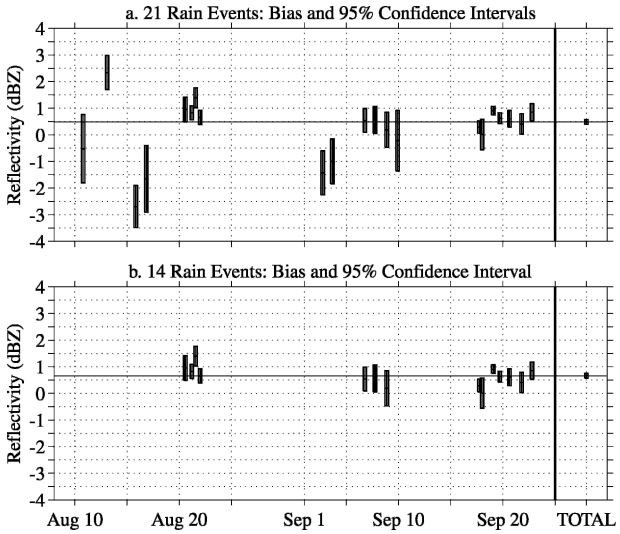

FIG. 9. (a) The statistics for each rain event; box symbols indicate the bias and the 95% confidence intervals. The ensemble statistics are shown on the far right of the plot. (b) The statistics for the 14 rain events selected because they have the least precipitation variation.

scanning radar observations. The 2062 simultaneous profiler and scanning radar observations below the bright band were analyzed as an ensemble and for each rain event. Several of the storms had statistics that deviated from the ensemble statistics. After evaluating the meteorological conditions of these outlier storms, it was determined that they were short-duration (about 30 min over the profiler) convective cells exhibiting large reflectivity variability quantified by the $\sigma_{5\text{min},630\text{m}}$ statistic. Ignoring these storms, the ensemble statistics suggested that the scanning radar was 0.66 dBZ higher than the profiler, the reflectivity difference standard deviation was 2.36 dBZ, and the 95% confidence interval was 0.09 dBZ. While the individual scanning radar to profiler comparisons show a large variation, the confidence interval about the mean bias is very small. There was very little variation in the bias statistic for each rainstorm, indicating that both radar systems were stable in their calibration during the TEFLUN-B campaign.

One advantage of comparing the reflectivity between two radar systems is that radar operators can determine if the calibration between the radars has changed with time. This could have an impact on short-term forecasts that rely on accurate calibrations to determine regions of potential hail and/or heavy rainfall and associated flash flooding. The comparison would provide a long-term record of the stability of both radar systems. This information could be implemented in a postcalibration processing to improve radar rainfall estimation. Long-term accurate estimates of areal rainfall are important for hydrologists to monitor water resources in their regions.

Since the location of the profiling and scanning radars usually do not change once they are deployed, the storm-to-storm and ensemble statistics can be easily automated and made graphically available. These products would become another tool that can be used to monitor the health and stability of the scanning radar. It needs to be stressed that the monitoring of the scanning radar does not require absolutely calibrating the profiling radar. The statistics can be calculated using the current calibration of both radar systems, and the change in statistics will be an indicator of a change in the performance of either radar system. The monitoring can be done in real time or during postcalibration analysis, depending on the resources and networking capabilities between the profiling and scanning radars.

Acknowledgments. This work has been partially supported by the NASA TRMM Project Office.

REFERENCES

Anagnostou, E. N., and W. F. Krajewski, 1998: Calibration of the WSR-88D precipitation processing subsystem. *Wea. Forecasting,* **13,** 396–406.

——, and ——, 1999a: Real-time radar rainfall estimation. Part I: Algorithm formulation. *J. Atmos. Oceanic Technol.,* **16,** 189–197.

——, and ——, 1999b: Real-time radar rainfall estimation. Part II: Case study. *J. Atmos. Oceanic Technol.,* **16,** 198–205.

——, ——, and J. Smith, 1999: Uncertainty quantification of mean-areal radar-rainfall estimates. *J. Atmos. Oceanic Technol.,* **16,** 206–215.

——, C. A. Morales, and T. Dinku, 2001: The use of TRMM precipitation radar observations in determining ground radar calibration biases. *J. Atmos. Oceanic Technol.,* **18,** 616–628.

Atlas, D., 2002: Radar calibration: Some simple approaches. *Bull. Amer. Meteor. Soc.,* **83,** 1313–1316.

——, P. Willis, and F. Marks, 1995: The effects of convective updrafts and downdrafts on reflectivity–rain rate relations and water budgets. Preprints, *27th Conf. on Radar Meteorology*, Vail, CO, Amer. Meteor. Soc., 19–22.

Austin, P. M., 1987: Relation between measured radar reflectivity and surface rainfall. *Mon. Wea. Rev.,* **115,** 1053–1070.

Baeck, M. L., and J. A. Smith, 1998: Rainfall estimation by the WSR-88D for heavy rainfall events. *Wea. Forecasting,* **13,** 416–436.

Baer, V. E., 1991: The transition from the present radar dissemination system to the NEXRAD Information Dissemination Service (NIDS). *Bull. Amer. Meteor. Soc.,* **72,** 29–33.

Bolen, S. M., and V. Chandrasekar, 2000: Quantitative cross validation of space-based and ground-based radar observations. *J. Appl. Meteor.,* **39,** 2071–2079.

Brandes, E. A., J. Vivekanandan, and J. W. Wilson, 1999: A comparison of radar reflectivity estimates of rainfall from collocated radars. *J. Atmos. Oceanic Technol.,* **16,** 1264–1272.

——, G. Zhang, and J. Vivekanandan, 2002: Experiments in rain-

fall estimation with a polarimetric radar in a subtropical environment. *J. Appl. Meteor.,* **41,** 674–685.

Bringi, V. N., and V. Chandrasekar, 2001: *Polarimetric Doppler Weather Radar*. Cambridge University Press, 636 pp.

Crum, T. D., and R. L. Alberty, 1993: The WSR-88D and the WSR-88D operational support facility. *Bull. Amer. Meteor. Soc.,* **74,** 1669–1688.

——, ——, and D. W. Burgess, 1993: Recording, archiving, and using WSR-88D data. *Bull. Amer. Meteor. Soc.,* **74,** 645–653.

——, R. E. Saffle, and J. W. Wilson, 1998: An update on the NEXRAD program and future WSR-88D support to operations. *Wea. Forecasting,* **13,** 253–262.

Fabry, F., 1996: On the determination of scale ranges for precipitation fields. *J. Geophys. Res.,* **101,** 12 819–12 826.

Gage, K. S., C. R. Williams, P. E. Johnston, W. L. Ecklund, R. Cifelli, A. Tokay, and D. A. Carter, 2000: Doppler radar profilers as calibration tools for scanning radars. *J. Appl. Meteor.,* **39,** 2209–2222.

——, W. L. Clark, C. R. Williams, and A. Tokay, 2004: Determining reflectivity measurement error from serial measurements using paired disdrometers and profilers. *Geophys. Res. Lett.,* **31,** L23107, doi:10.1029/2004GL020591.

Glitto, P., and B. Choy, 1997: A comparison of WSR-88D storm total precipitation performance during two tropical systems following changes to the multiplicative bias and upper reflectivity threshold. *Wea. Forecasting,* **12,** 459–471.

Heiss, W. H., D. L. McGrew, and D. Sirmans, 1990: NEXRAD: Next Generation Weather Radar (WSR-88D). *Microwave J.,* **33,** 79–98.

Houze, R. A., Jr., 1993: *Cloud Dynamics*. Academic Press, 573 pp.

Joss, J., and A. Waldvogel, 1969: Raindrop size distribution and sampling. *J. Atmos. Sci.,* **26,** 566–569.

Martner, B. E., 1977: A field experiment on the calibration of radars with raindrop disdrometers. *J. Appl. Meteor.,* **16,** 451–454.

May, P. T., A. R. Jameson, T. D. Keenan, and P. E. Johnston, 2001: A comparison between polarimetric radar and wind profiler observations of precipitation in tropical showers. *J. Appl. Meteor.,* **40,** 1702–1717.

——, ——, ——, ——, and C. Lucas, 2002: Combined wind profiler/polarimetric radar studies of the vertical motion and microphysical characteristics of tropical sea-breeze thunderstorms. *Mon. Wea. Rev.,* **130,** 2228–2239.

Ralph, F. M., 1995: Using radar-measured radial vertical velocities to distinguish precipitation scattering from clear-air scattering. *J. Atmos. Oceanic Technol.,* **12,** 257–267.

Serafin, R. J., and J. W. Wilson, 2000: Operational weather radar in the United States: Progress and opportunity. *Bull. Amer. Meteor. Soc.,* **81,** 501–518.

Sheppard, B. E., and P. I. Joe, 1994: Comparison of raindrop size distribution measurements by a Joss-Waldvogel disdrometer, a PMS 2DG spectrometer, and a POSS Doppler radar. *J. Atmos. Oceanic Technol.,* **11,** 874–887.

Smith, J. A., D.-J. Seo, M. L. Baeck, and M. D. Hudlow, 1996: An intercomparison study of NEXRAD precipitation estimates. *Water Resour. Res.,* **32,** 2035–2045.

Smith, P. L., Z. Liu, and J. Joss, 1993: A study of sampling-variability effects in raindrop size observations. *J. Appl. Meteor.,* **32,** 1259–1269.

Srivastava, R. C., 1987: A model of intense downdrafts driven by the melting and evaporation of precipitation. *J. Atmos. Sci.,* **44,** 1752–1773.

Stellman, K. M., H. E. Fuelberg, R. Garza, and M. Mullusky, 2001: An examination of radar and rain gauge–derived mean areal precipitation over Georgia watersheds. *Wea. Forecasting,* **16,** 133–144.

Ulbrich, C. W., and L. G. Lee, 1999: Rainfall measurement error by WSR-88D radars due to variations in *Z–R* law parameters and the radar constant. *J. Atmos. Oceanic Technol.,* **16,** 1017–1024.

——, and N. E. Miller, 2001: Experimental test of the effects of *Z–R* law variations on comparison of WSR-88D rainfall amounts with surface rain gauge and disdrometer data. *Wea. Forecasting,* **16,** 369–375.

Williams, C. R., W. L. Ecklund, P. E. Johnston, and K. S. Gage, 2000: Cluster analysis techniques to separate air motion and hydrometeors in vertical incident profiler observations. *J. Atmos. Oceanic Technol.,* **17,** 949–962.